RESEARCH ARTICLE

8-Triazolylpurines: Towards Fluorescent Inhibitors of the MDM2/p53 Interaction

Mariell Pettersson[1☯], David Bliman[1☯], Jimmy Jacobsson[1], Jesper R. Nilsson[2], Jaeki Min[3], Luigi Iconaru[4], R. Kiplin Guy[3], Richard W. Kriwacki[4], Joakim Andréasson[2], Morten Grøtli[1] *

1 Department of Chemistry and Molecular Biology, University of Gothenburg, Gothenburg, Sweden, 2 Department of Chemical and Biological Engineering/Chemistry and Biochemistry, Chalmers University of Technology, Gothenburg, Sweden, 3 Department of Chemical Biology and Therapeutics, St. Jude Children's Research Hospital, 262 Danny Thomas Place, Memphis, Tennessee, United States of America, 4 Department of Structural Biology, St. Jude Children's Research Hospital, 262 Danny Thomas Place, Memphis, Tennessee, United States of America

☯ These authors contributed equally to this work.
* grotli@chem.gu.se

Abstract

Small molecule nonpeptidic mimics of α-helices are widely recognised as protein-protein interaction (PPIs) inhibitors. Protein-protein interactions mediate virtually all important regulatory pathways in a cell, and the ability to control and modulate PPIs is therefore of great significance to basic biology, where controlled disruption of protein networks is key to understanding network connectivity and function. We have designed and synthesised two series of 2,6,9-substituted 8-triazolylpurines as α-helix mimetics. The first series was designed based on low energy conformations but did not display any biological activity in a biochemical fluorescence polarisation assay targeting MDM2/p53. Although solution NMR conformation studies demonstrated that such molecules could mimic the topography of an α-helix, docking studies indicated that the same compounds were not optimal as inhibitors for the MDM2/p53 interaction. A new series of 8-triazolylpurines was designed based on a combination of docking studies and analysis of recently published inhibitors. The best compound displayed low micromolar inhibitory activity towards MDM2/p53 in a biochemical fluorescence polarisation assay. In order to evaluate the applicability of these compounds as biologically active and intrinsically fluorescent probes, their absorption/emission properties were measured. The compounds display fluorescent properties with quantum yields up to 50%.

Introduction

Protein-protein interactions (PPIs) mediate virtually all important biological regulatory pathways [1], and the ability to control and modulate PPIs is therefore of great significance to basic biology, where the controlled disruption of PPI networks is key to understanding network

connectivity and function. It is also becoming increasingly clear that the modulation of PPIs offers enormous opportunities in drug discovery for medical diagnostics and treatment.

Designing small molecule inhibitors of PPIs poses a substantial challenge due to PPIs generally shallow interaction sites and large surface area as compared with more traditionally targeted enzyme active sites [2]. However, small regions consisting of a collection of residues that constitute the majority of the free binding energy have been identified and are generally referred to as "hot spots" [3]. These hot spots are often amino acid residues protruding from one face of an α-helix at the interaction surface [4]. A mimetic that reproduces the key interactions of the α-helix should bind to the target binding site of the α-helix.

Tumour protein p53 is crucial in multicellular organisms, where it regulates the cell cycle and functions as a tumour suppressor [5, 6]. All known tumour cells either mutate the p53 gene, or use internal cell p53 modulators like MDM2 and MDMX to disable its function. Releasing functional p53 from inhibition by MDM2 and MDMX should, in principle, provide an efficient, nongenotoxic means of cancer therapy.

The p53 protein binds to MDM2 and MDMX using a short helix with a "hot spot triad" consisting of p53's Trp23, Leu26, and Phe19 [7]. A number of elegant examples of nonpeptidic α-helix mimetics that inhibit the MDM2/p53 interaction by targeting these hot spots have been published [8]. These inhibitors can be divided into three subcategories: type I, II and III [9]. Type I inhibitors include stabilised oligomers that are designed to mimic the α-helical topography. The second type of inhibitors, functional mimetics, are based on scaffolds that place substituents in the spatial orientation of the parent helix, but the scaffolds themselves are not designed to mimic the α-helix topography. Notable examples of type II inhibitors include the nutlins [10], piperidinones [11] and spiroindolines [12]. These scaffolds vary widely in structure but share the common denominator that they can arrange the substituents in analogy with the i, $i+4$ and $i+7$ amino acid side chains of an α-helical structure. In the third category of inhibitors, the nonpeptidic scaffold mimics the topography of an α-helix with substituents protruding in the positions of the i, $i+4$ and $i+7$ amino acid side chains of an α-helical structure. Examples from type III include terphenyl [13, 14], and 8-amido-pyrrolopyrimidines[15].

Purines widely occur in nature [16] and are recognised as privileged structures in drug discovery [17]. We have previously developed 8-(triazolyl) purines as fluorescent base analogues [18, 19] and hypothesised that 8-(triazolyl)purines with substituents in the 2- and 9-positions would project their substituents in analogy with the residues of one face of an α-helix (Fig 1). 7-Deazapurines have previously been reported as inhibitors for MDM2/p53 [15]. Since triazoles are recognised as bioisosters of amide bonds [20–22], we chose to evaluate 8-(triazolyl) purines as α-helix mimetics. Furthermore, given the fluorescent properties of 8-triazolylpurines that were previously reported by our group, we expected 2,9-substituted 8-triazolylpurines to display similar characteristics. Compounds that display both biological activity and intrinsically fluorescent properties would be extremely useful for all applications in which intracellular localisation of the bio-relevant molecule is of interest.

Here, we have evaluated a series of 2,9-substituted 8-(triazolyl)purines as α-helix mimetics. The UV/vis absorption and fluorescence properties of these compounds have also been characterised.

Results and Discussion

Type III inhibitors

Design. Comparison of low energy conformations of 8-(triazolyl)purine derivatives with an idealised α-helix (Fig 1c) indicated that the scaffold arranges substituents in the N2, 9 and on the triazole analogous to the i, $i+4$, $i+7$ residues (Fig 1).
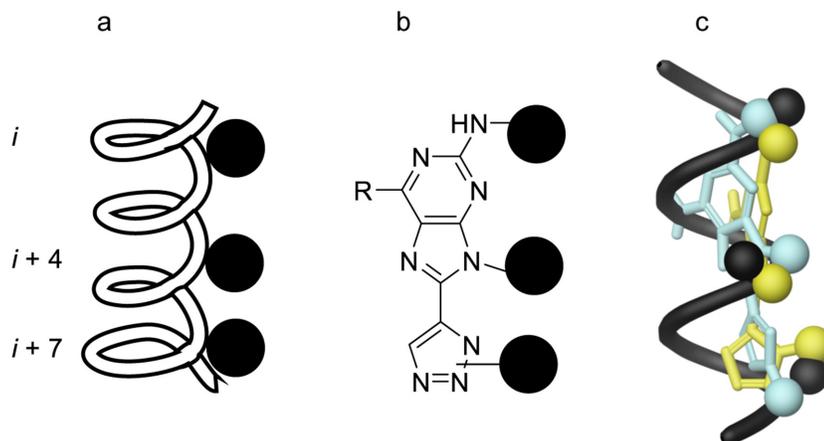
Fig 1. Overview of 8-(triazolyl)purine design. Schematic representation of a) an α-helix with residues present on one face of the helix (*i*, *i*+4 and *i*+7) denoted as black spheres, and b) the 8-triazolyl scaffold with R-groups denoted as black spheres. c) Superimposition of Ala-helix (black), with low energy conformations of 8-(1,4-triazolyl)-purine (turquoise) and 8-(1,5-triazolyl)-purine (yellow).

doi:10.1371/journal.pone.0124423.g001

The regiochemistry of the triazole can be controlled by the choice of catalyst, which provides a possibility to access compounds with structural diversity. Performing the cyclisation in the presence of a Cu(I) catalyst results in the 1,4-triazole [23]. Changing the catalyst system to Ru (II) results in the 1,5-triazole with high regioselectivity [24]. The 1,5-regioisomer can alternatively be obtained with $Me_4N^+OH^-$ as catalyst in DMSO [25]. Alkyl- and benzylazides can be obtained from readily available alkylhalides, enabling chemical diversity for the introduction of the R_3 substituent. The terminal alkyne required for the cyclisation could be accessible through a palladium-catalyzed Sonagashira-type C-C coupling. Activation of the 8-position with a halide would set it up for the C-C coupling. The R_4 substituent was intended to be introduced by a nucleophilic aromatic substitution (S_NAr). The precedence in the literature [26] for this type of reaction in the 6-position of purine derivatives and the commercial availability of 6-chloro-purines made this strategy a reasonable choice. Possible strategies for the introduction of substituents in the *N*2 and 9-positions include nucleophilic substitution of alkyl halides, reductive amination (*N*2) or alternatively Mitsunobu-type reactions with primary and secondary alcohols.

Synthesis. The *i*, *i*+4 and *i*+7 residues on the α-helix of p53, that are generally recognised as key residues for MDM2 binding, are all hydrophobic (leucine, tryptophan and phenylalanine), which led to the selection of a series of hydrophobic substituents in R_{1-3} for our compounds. The initial route to 2,6,8,9-substituted purines started with alkylation of the 9 position using alkyl or benzyl halide followed by the introduction of a substituent in the *N*2 position via reductive amination. While the alkylation in the 9-position produced reasonable yields using 3-bromo-2-methylpropene (73%), benzyl bromide (59%) and phenethyl bromide (93%) [27], the reductive amination using $NaCNBH_3$ or $NaBH(OAc)_3$ failed due to the low reactivity of the 2-amino substituent. The major product generated in the reaction was the alcohol product from reduction of the corresponding aldehyde. We then turned to alkylation of the *N*2 position despite expected problems with bis-substitution. As expected, alkylation with aryl halides, potassium iodide and potassium carbonate as base at *N*2 resulted in a mixture of mono- and bis-substitution. Although these species were easily separated by column chromatography, this route failed to generate sufficient quantities of the 2,9-substituted intermediate. It was therefore decided to investigate alternative strategies to achieve these substitutions.
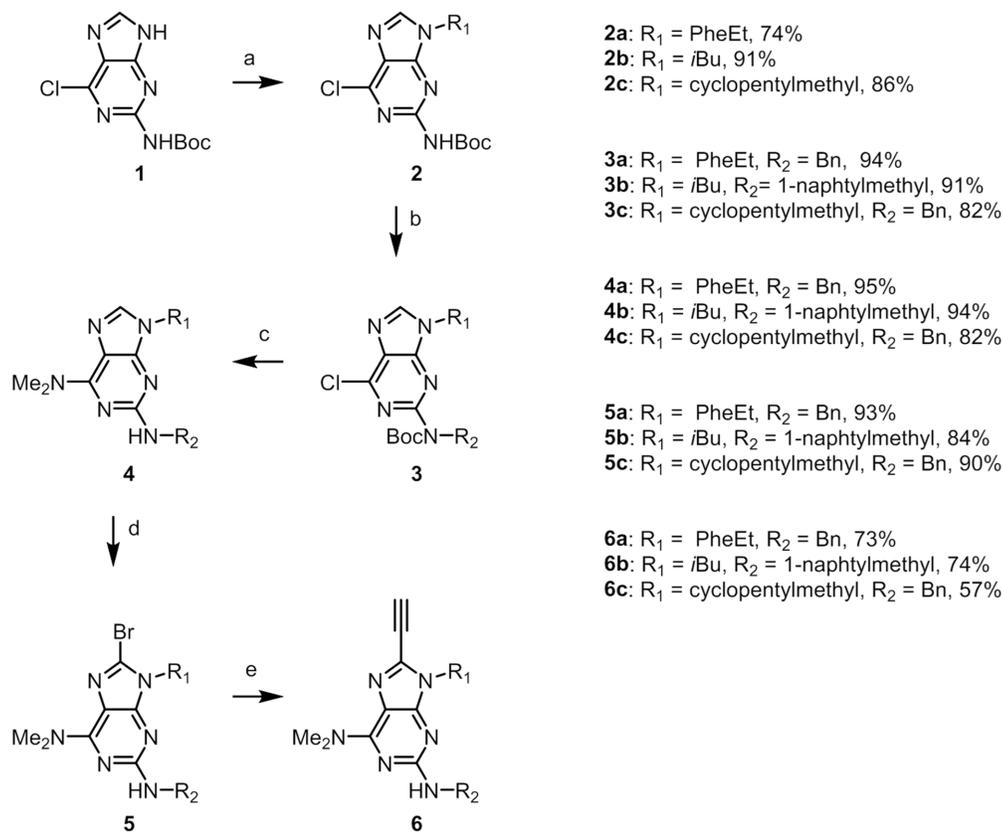
Fig 2. Synthesis of compound 1–6. Reaction conditions: (**a**) R$_1$OH, DIAD, Ph$_3$P, THF. (**b**) R$_2$OH, ADDP, *n*Bu$_3$P, THF. (**c**) DMF, MW, 180°C. (**d**) PyBr$_3$, CH$_2$Cl$_2$. (**e**) (i) Pd(II)Cl$_2$(PPh$_3$)$_2$, Cu(I)I, Amberlite IRA-67, TMS-acetylene, MW, 110°C. (ii) PS-F, THF.
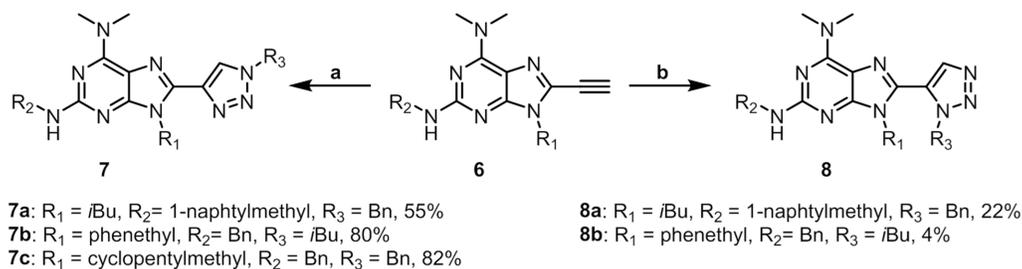
doi:10.1371/journal.pone.0124423.g002

Fletcher et al. have published a synthesis of 2,9-substituted guanines starting from 6-chloro-2-amino-purine [28, 29]. The synthesis involves Boc protection in the *N*2-position (**1**) in order to activate it for Mitsunobu coupling (Fig 2). The regioselectivity in the two consecutive Mitsunobu couplings relies on the greater reactivity of the 9-position. This protocol proved successful and allowed us to gain access to **3a-c**. Yields were typically high in both couplings, ranging from 74–91% (**2a-c**) for reactions in the 9-position and 82–94% (**3a-c**) on the exocyclic *N*2-amine.

The chloro substituent in the 6-position of compound **3** is susceptible to nucleophilic aromatic substitution (Fig 2). The dimethylamino substituent was introduced by heating **3a-e** in DMF at 180°C [30]. These reaction conditions also remove the Boc protecting group in the *N*2-position, resulting in **4a-c** in 82–95% yield.

Regarding the next step, activating the 8-position towards C-C-cross coupling by introduction of a bromide, we recently published a procedure for 8-bromination of electron-rich purine derivative using PyBr$_3$ in DCM [27]. This procedure afforded **5a-e** in high yields, between 84 and 93%. It is worth mentioning that the bromination is regiospecific and does not react with aromatic substituents.

The terminal alkyne needed for the cyclization was introduced by a Sonogashira-type C-C cross coupling catalysed by PdCl$_2$(PPh$_3$)$_2$ and CuI. Using a solid supported tertiary amine (Amberlite^{TM} IRA67) as base facilitates the workup, and deprotection of the trimethylsilyl group can be carried out on the crude product after filtration to remove the base. Trimethylsilyl

Fig 3. Synthesis of 7a-c and 8a-b. Reaction conditions: (**a**) NaN$_3$, R$_3$-X, Cu(I)I, NaAsc, DMEDA, DMF. (**b**) Cp*RuCl(PPh$_3$)$_2$, MW, 120°C, DMF.

doi:10.1371/journal.pone.0124423.g003

removal using polymer supported fluoride (PS-F) in THF afforded **6a-e** in yields of 57–74% over two steps (Fig 2). Here again, the use of a polymer-supported reagent facilitates the work-up of the reaction.

1,4-triazoles can be formed with high regioselectivity using a Cu(I) catalyst, a reaction referred to as Copper Catalysed Azide Alkyne Cyclisation (CuAAC). **7a** was obtained by reacting alkyne **6b** with benzyl azide in the presence of CuI, sodium ascorbate and DMEDA at room temperature overnight (Fig 3). To avoid the need to isolate low molecular weight, potentially explosive alkyl azides, isobutyl azide was formed immediately prior to use from isobutyl bromide and sodium azide in DMF. Alkyne, CuI, sodium ascorbate and DMEDA were then added to the azide solution. 1,4-triazolepurines **7a–c** were isolated in 55–82% yields (Fig 3). 1,5-Triazoles are accessible by ruthenium-catalysed cyclisation of azides and alkynes [24] and a method for sequential preformation of low molecular weight azides has been reported [31]. Reacting alkyne **6b** with benzyl azide afforded **8a** in 22% yield and when 1,5 cyclization with iso-butylazide was attempted, the expected product (**8b**) was isolated in very low yield after extensive purification (Fig 3). The low yield can be attributed, at least in part, to difficulties in separating the product from unidentified by-products.

Evaluation against MDM2/p53. Compounds **7a-c** and **8a-b** were evaluated as MDM2 inhibitors in a fluorescence polarisation (FP) assay that measures displacement of a wild-type p53 peptide tagged with a fluorescent probe (Texas Red) bound to MDM2. Unfortunately, the compounds showed no activity at the concentrations tested (up to 47 μM). However, these results prompted us to investigate the solution conformation.

Solution conformation analysis. The ability of 8-triazolylpurines to act as α-helix mimetics is dependent on the conformation of the triazole moiety in relation to the purine since this determines the relative positions of the R$_1$ and R$_3$ substituents. The conformation of **8a** in solution was determined by a combined NMR spectroscopic and computational analysis utilizing the NMR Analysis of Molecular Flexibility (NAMFIS) algorithm [32]. NAMFIS has previously been employed for description of the solution conformations of oligopeptides [33] and small molecules [34], and to evaluate the effect of interstrand hydrogen bonding on β-hairpin stability of cyclic peptides [35]. Experimental proton-proton distances were derived from a NOESY buildup using the initial rate approximation with five mixing times between 80 and 800 ms, ensuring linearity. Theoretically available conformations were predicted using Monte Carlo conformational searches along with Molecular Mechanics Minimisation (MCMM). In order to ensure that the entire conformational space available for the compound was sampled, the conformational search was performed with two different force fields (Amber* and OPLS-2005) and three different solvent models (chloroform, water and octanol). The conformational ensembles were combined and the redundant conformations were removed. Using the NAMFIS algorithm the conformations existing in solution were selected based on the experimentally obtained distances (NOE).
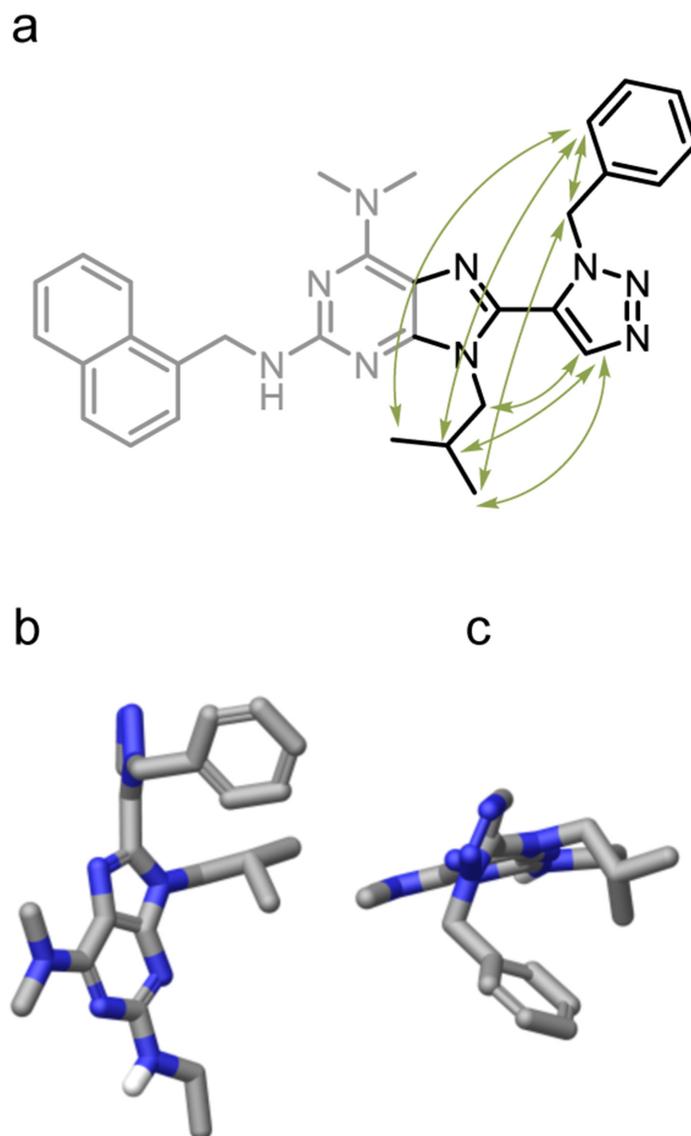
Fig 4. Conformational analysis of 8a. a) NOE correlations (green arrows) in proximity of the triazole ring observed for **8a**. b) Sideview and c) topview of one of the conformations found in the NAMFIS-analysis. (All 6 NAMFIS conformations can be found in Fig. D and E in S1 File).

doi:10.1371/journal.pone.0124423.g004

NAMFIS analysis identified an ensemble of 6 conformations in solution, including conformations that place the substituent in the same spatial orientation as the side chains of an idealised α-helix (Fig 4). The R_2 substituent was omitted from the analysis since the goal of the conformation analysis was to determine the distance and relative orientation of the R_1 and R_3 substituents. The distance and orientation between R_2 and R_1 is determined by the rigid and flat purine ring system. An analysis of this part of the molecule would add little or no information about the relative positions of the R_1 and R_3 substituents.

The solution conformations for the 1,4-regioisomer (**7a**) were elucidated using the same method. The experimental distances between protons on the triazole ring and the R_1 and R_3 substituents (see Fig 5) were determined by running NOE-buildups with 5 mixing times (80, 200, 400, 600, 800 and 1000 ms). As only two NOE correlations from the triazole H-X are
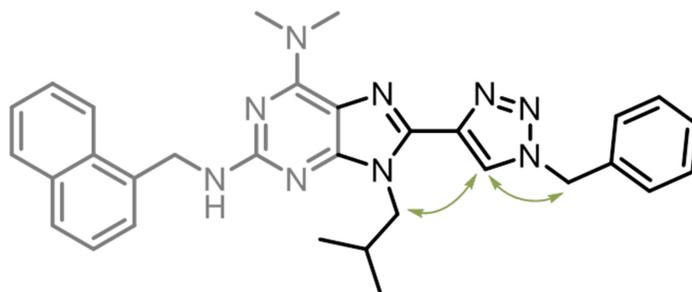
Fig 5. NOE correlations observed for 7a. NOE correlations in proximity of the triazole ring observed for **7a**.

observed for the 1,4-regioisomer ([Fig 5](#)), the conformational ensemble could not be reliably determined (overfitting).

The aqueous solubility of compound **7c** was measured and shown to be low (0.3 μM at pH 7.4). Although these compounds are suspected (and supposed) to be lipophilic, the solubility was too low to be practical for biological studies. A more hydrophilic substituent in the 6-position could increase the aqueous solubility of the compounds.

In summary, the solution conformational studies showed that the 8-triazolylpurines scaffold should be able to place the R_1 and R_3 substituents in a spatial orientation that mimics the α-helical conformation. The analysis did not, however, reveal why this series was inactive against MDM2/p53 in the FP assay. Since the compounds were inactive as inhibitors against MDM2/p53 interaction at the concentrations evaluated and also showed poor solubility, re-evaluation of the design was undertaken, opting for type II inhibitors.
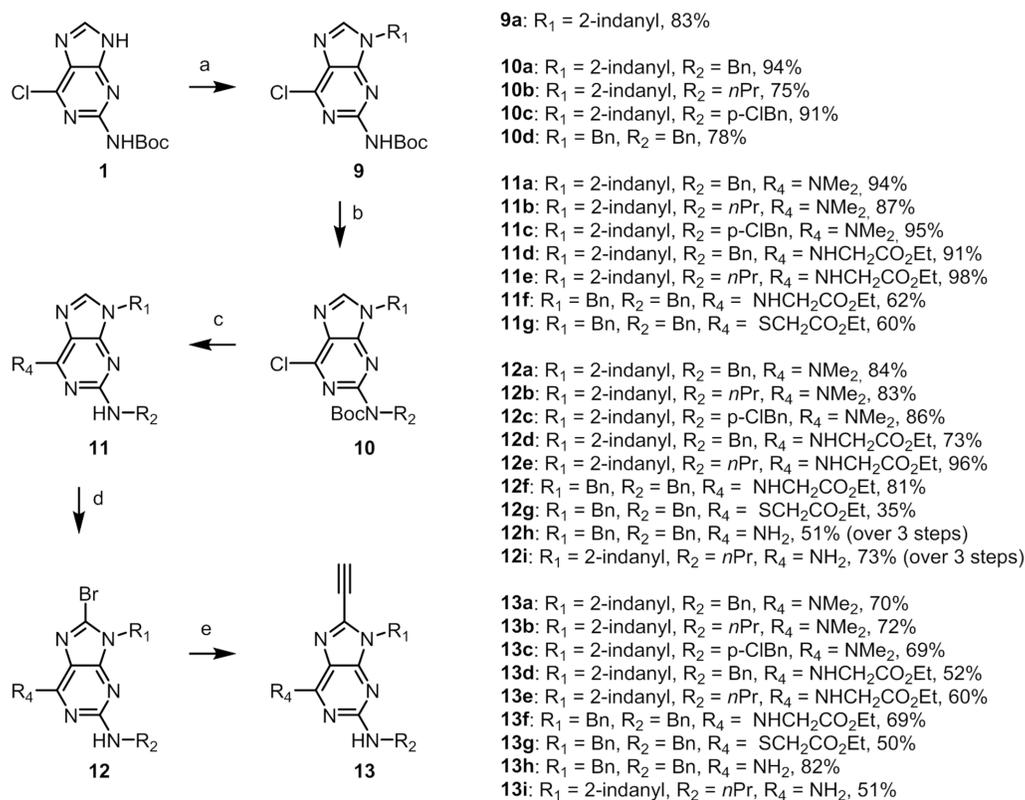
Type II inhibitors

Design. During our work with the 8-triazolylpurines, new crystal structures of MDM2 co-crystallised with highly potent inhibitors were published [11, 36–38]. Analysis of these and previously published crystal structures [10] of ligand/MDM2 complexes encouraged us to examine two main changes in our design. First, the size of one or two of the hydrophobic substituents should be decreased. Second, several of the published binders of MDM2 have a hydrophilic substituent pointing out towards the solvent/hydrophilic surface of MDM2 enabling hydrogen bonding and/or ionic interactions with the His96 and Lys94 residues of MDM2. The 6-position of our purine derivatives was suitable for the introduction of such functional groups. A series of 8-(triazolyl)purine derivatives were docked into the α-helix binding site of MDM2 (PDB code: 4HBM), using the Schrödinger software package (Glide XP mode), to find a suitable substitution pattern on the 8-(triazolyl)purine ring system. This crystal complex was chosen due to the high affinity and potency of the co-crystallized piperidinones. The models suggest that decreasing the size of the R_3 substituent to a methyl group, R_2 to a propyl and R_1 to an indanyl should improve the fit between the ligand and MDM2. The indanyl is a more rigid isoster of phenethyl. In addition, the introduction of a more hydrophilic group such as an acid or ester could give rise to hydrogen bonding and/or ionic interactions. An example where R_1 = indanyl, R_2 = propyl, R_3 = methyl, and R_4 = NHCH$_2$COOH is shown in [Fig 6b](#). A series of purines with R_{1-3} substituents with varying size and shape were selected for further evaluation of inhibitors. Compound **8a** (type III) was also docked in the grid built from the ligand binding site of MDM2 (PDB code: 4HBM). As expected, the R_{1-3} substituents of a type III inhibitor do not fit into Phe-Trp-Leu-pockets of a crystal structure derived from a type II inhibitor/MDM2 complex.
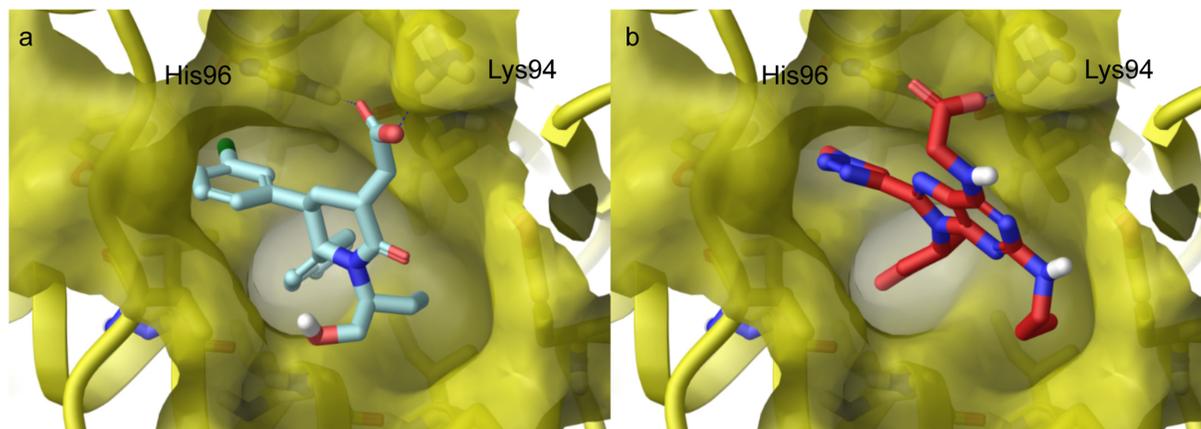
Fig 6. Small molecule inhibitors bound to MDM2. a) Crystal structure of a piperidinone-based inhibitor bound to MDM2 (PDB code: 4HBM)[37] and b) type II inhibitor (R_1 = indanyl, R_2 = propyl, R_3 = methyl and R_4 = $NHCH_2COOH$) docked into the MDM2 binding site.

doi:10.1371/journal.pone.0124423.g006

The syntheses of our second series of compounds are shown in Fig 7 Introduction of R_1 and R_2 substituents and dimethylamine in the 6-position was performed as described above; **10a-d** and **11a-b** were isolated in 75–94% and 87–94% yield, respectively. When the *N*2-position was substituted with a *p*-chlorobenzyl, milder conditions for the introduction of dimethylamine
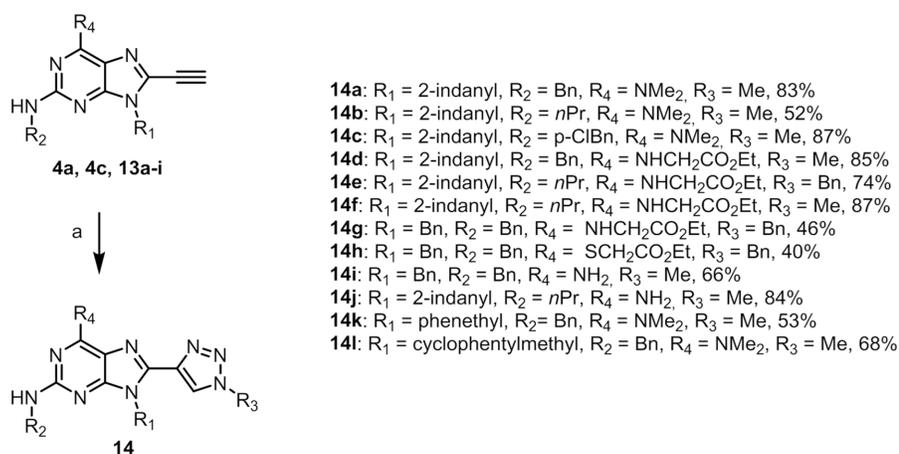

9a: R_1 = 2-indanyl, 83%

10a: R_1 = 2-indanyl, R_2 = Bn, 94%
10b: R_1 = 2-indanyl, R_2 = *n*Pr, 75%
10c: R_1 = 2-indanyl, R_2 = p-ClBn, 91%
10d: R_1 = Bn, R_2 = Bn, 78%

11a: R_1 = 2-indanyl, R_2 = Bn, R_4 = NMe_2, 94%
11b: R_1 = 2-indanyl, R_2 = *n*Pr, R_4 = NMe_2, 87%
11c: R_1 = 2-indanyl, R_2 = p-ClBn, R_4 = NMe_2, 95%
11d: R_1 = 2-indanyl, R_2 = Bn, R_4 = $NHCH_2CO_2Et$, 91%
11e: R_1 = 2-indanyl, R_2 = *n*Pr, R_4 = $NHCH_2CO_2Et$, 98%
11f: R_1 = Bn, R_2 = Bn, R_4 = $NHCH_2CO_2Et$, 62%
11g: R_1 = Bn, R_2 = Bn, R_4 = SCH_2CO_2Et, 60%

12a: R_1 = 2-indanyl, R_2 = Bn, R_4 = NMe_2, 84%
12b: R_1 = 2-indanyl, R_2 = *n*Pr, R_4 = NMe_2, 83%
12c: R_1 = 2-indanyl, R_2 = p-ClBn, R_4 = NMe_2, 86%
12d: R_1 = 2-indanyl, R_2 = Bn, R_4 = $NHCH_2CO_2Et$, 73%
12e: R_1 = 2-indanyl, R_2 = *n*Pr, R_4 = $NHCH_2CO_2Et$, 96%
12f: R_1 = Bn, R_2 = Bn, R_4 = $NHCH_2CO_2Et$, 81%
12g: R_1 = Bn, R_2 = Bn, R_4 = SCH_2CO_2Et, 35%
12h: R_1 = Bn, R_2 = Bn, R_4 = NH_2, 51% (over 3 steps)
12i: R_1 = 2-indanyl, R_2 = *n*Pr, R_4 = NH_2, 73% (over 3 steps)

13a: R_1 = 2-indanyl, R_2 = Bn, R_4 = NMe_2, 70%
13b: R_1 = 2-indanyl, R_2 = *n*Pr, R_4 = NMe_2, 72%
13c: R_1 = 2-indanyl, R_2 = p-ClBn, R_4 = NMe_2, 69%
13d: R_1 = 2-indanyl, R_2 = Bn, R_4 = $NHCH_2CO_2Et$, 52%
13e: R_1 = 2-indanyl, R_2 = *n*Pr, R_4 = $NHCH_2CO_2Et$, 60%
13f: R_1 = Bn, R_2 = Bn, R_4 = $NHCH_2CO_2Et$, 69%
13g: R_1 = Bn, R_2 = Bn, R_4 = SCH_2CO_2Et, 50%
13h: R_1 = Bn, R_2 = Bn, R_4 = NH_2, 82%
13i: R_1 = 2-indanyl, R_2 = *n*Pr, R_4 = NH_2, 51%

Fig 7. Synthesis of 9–13. Reaction conditions: (**a**) R_1OH, DIAD, Ph_3P, THF. (**b**) R_2OH, ADDP, nBu_3P, THF. (**c**) R_4 = NMe_2, DMF, MW, 180°C. R_2 = *p*-ClBn, R_4 = NMe_2, (i) 5.6 M NMe_2 in ethanol. (ii) TFA/CH_2Cl_2. R_4 = $NHCH_2CO_2Et$, (i) $NH_2CH_2CO_2Et$, Et_3N, ethanol, 100°C. (ii) TFA/CH_2Cl_2, R_4 = SCH_2CO_2Et, (i) $SHCH_2CO_2Et$, NaH, toluene, 70°C. (ii) TFA/CH_2Cl_2. (**d**) $PyBr_3$, CH_2Cl_2. For R_4 = NH_2, (i) NH_4OH (aq.), dioxane, 100°C. (ii) TFA/CH_2Cl_2 (iii) $PyBr_3$, CH_2Cl_2. (**e**) (i) $Pd(II)Cl_2(PPh_3)_2$, Cu(I)I, Amberlite IRA-67, TMS-acetylene, MW, 110°C. (ii) PS-F, THF.

doi:10.1371/journal.pone.0124423.g007

were used to avoid aromatic substitution in the *p*-chloro position. Running the reaction with dimethylamine in ethanol (5.6 M) at 80°C gave regioselective substitution of the 6-chloro and subsequent Boc removal with TFA in DCM gave **11c** in 95% yield over two steps. For the introduction of an ester in the 6-postion, the 6-chloropurine derivatives were reacted with thioglycol ethylester and glycine ethylester under basic conditions followed by Boc removal (TFA/DCM) to give **11d-g** in 60–98% yields over two steps. Next, treatment of **11a-g** with PyrBr$_3$ provided **12a-g** in 35–96% yield, where the lower yields of 35% was obtained for bromination of compound **11g**. Sulphur in the 6-position gives lower yields compared with nitrogen. An alternative to decrease the lipophilicity of these compounds would be to introduce a primary amine in the 6-position. Treatment of the 6-chloroderivatives with ammonium hydroxide gave the 6-aminoderivative. Bromination using PyBr$_3$ in DCM did not give the desired product which was assumed to be due to the electron withdrawing effect of the Boc group in the *N*2-position. Removing the Boc group with TFA in DCM prior to the bromination was necessary to facilitate the success of the reaction. The amination, deprotection and bromination sequence can be run conveniently without any intermediate purification to afford **12h** and **12i** in 51 and 73% yield over three steps, respectively.

The Sonsogashira coupling followed the same protocol as above to give **13a-i** (Fig 7). Further, the same protocol for the 1,4-triazole formation was again employed to provide **14a-l** (Fig 8), and as described above for the synthesis of isobutylazide, methylazide was formed *in situ*. The highest yields in the cyclisation were obtained when the azide formation was run in room temperature followed by cyclisation at 60°C. Low yields were isolated if the reaction mixture vial was flushed with nitrogen after azide formation which is assumed to be due to the volatility of methylazide.

These new compounds were also evaluated for their inhibitory effect on MDM2 in a fluorescence polarisation assay. Of the 12 new compounds, 10 were inactive towards p53/MDM2 at concentrations up to 100 μM. Compounds **14f** and **14j** (Fig 9) displayed IC$_{50}$ values of 10 (Fig. P in S1 File) and 56 μM, respectively. Compound **14f** was further evaluated using Water-LOGSY[39] which confirmed binding to MDM2 (Fig. Q in S1 File). These results verify that with this scaffold, compounds with larger substituents in the R$_1$ and R$_2$-position do not bind to MDM2. This validates the redesign and fits with the observation that many of the published low nM inhibitors of the p53/MDM2 interaction are typically less extended than the model p53 α-helix. One explanation for the low potency observed for the type II 8-(triazolyl)purine

4a, 4c, 13a-i

a

14

14a: R$_1$ = 2-indanyl, R$_2$ = Bn, R$_4$ = NMe$_2$, R$_3$ = Me, 83%
14b: R$_1$ = 2-indanyl, R$_2$ = *n*Pr, R$_4$ = NMe$_2$, R$_3$ = Me, 52%
14c: R$_1$ = 2-indanyl, R$_2$ = p-ClBn, R$_4$ = NMe$_2$, R$_3$ = Me, 87%
14d: R$_1$ = 2-indanyl, R$_2$ = Bn, R$_4$ = NHCH$_2$CO$_2$Et, R$_3$ = Me, 85%
14e: R$_1$ = 2-indanyl, R$_2$ = *n*Pr, R$_4$ = NHCH$_2$CO$_2$Et, R$_3$ = Bn, 74%
14f: R$_1$ = 2-indanyl, R$_2$ = *n*Pr, R$_4$ = NHCH$_2$CO$_2$Et, R$_3$ = Me, 87%
14g: R$_1$ = Bn, R$_2$ = Bn, R$_4$ = NHCH$_2$CO$_2$Et, R$_3$ = Bn, 46%
14h: R$_1$ = Bn, R$_2$ = Bn, R$_4$ = SCH$_2$CO$_2$Et, R$_3$ = Bn, 40%
14i: R$_1$ = Bn, R$_2$ = Bn, R$_4$ = NH$_2$, R$_3$ = Me, 66%
14j: R$_1$ = 2-indanyl, R$_2$ = *n*Pr, R$_4$ = NH$_2$, R$_3$ = Me, 84%
14k: R$_1$ = phenethyl, R$_2$= Bn, R$_4$ = NMe$_2$, R$_3$ = Me, 53%
14l: R$_1$ = cyclophentylmethyl, R$_2$ = Bn, R$_4$ = NMe$_2$, R$_3$ = Me, 68%

Fig 8. Synthesis of 14a-l. Reaction conditions: (**a**) NaN$_3$, R$_3$-X, Cu(I)I, NaAsc, DMEDA, DMF.

doi:10.1371/journal.pone.0124423.g008

14f   **14j**
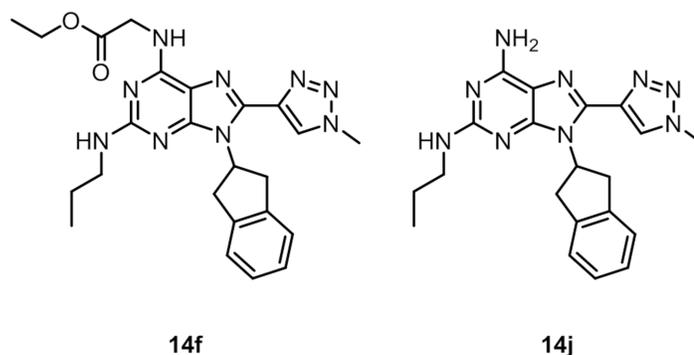
Fig 9. 8-(triazolyl)purine inhibitors of MDM2/p53.

doi:10.1371/journal.pone.0124423.g009

derivatives could be that while the methyl on the triazole fits into one of the hydrophobic interaction sites as observed in the docking studies, this fit might bury the polar triazole as well, resulting in a desolvation penalty. Furthermore, the active compounds **14f** and **14j** lack the ability of the ionic interaction formed between the carboxylic acid of the model inhibitor (piperidinones) and the Lys94 residue of MDM2. Recently published docking studies of known p53/MDM2 inhibitors highlight the challenges posed by using docking as a tool for developing inhibitors against this target.[40]
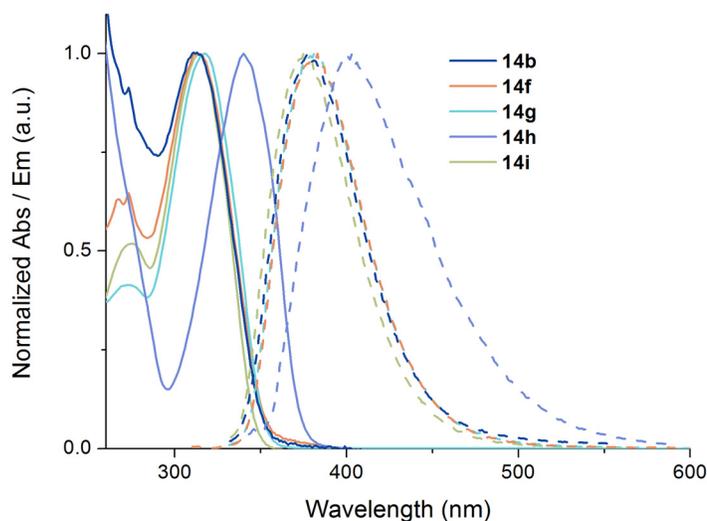
Photophysical characterisation. Intrinsically fluorescent α-helix mimetics could be used for imaging and localization of the compounds in cells. We have previously reported the fluorescent properties of 6,9-substituted 8-triazolylpurines [18] and anticipated that the structurally similar 2,6,9-substituted derivatives would have similar behaviour. UV/vis absorption and fluorescence measurements were undertaken to investigate this possibility. The data are presented in Table 1.

Table 1. Absorption and fluorescent properties of 8-(triazolyl)purine derivatives in methanol solution.

Entry	Compound	R_1	R_2	R_3	R_4	$\lambda_{abs,max}$ (nm)	$\lambda_{em,max}$ (nm)	Φ_F (%)
1	**14a**	2-indanyl	Bn	1,4-Me	NMe_2	310	376	2
2	**14k**	phenethyl	Bn	1,4-Me	NMe_2	315	376	2
3	**7c**	cyclopentylmethyl	Bn	1,4-Bn	NMe_2	317	377	2
4	**14b**	2-indanyl	nPr	1,4-Me	NMe_2	311	378	1
5	**14l**	cyclopentylmethyl	Bn	1,4-Me	NMe_2	316	376	2
6	**14i**	Bn	Bn	1,4-Me	NH_2	314	375	7
7	**14j**	2-indanyl	nPr	1,4-Me	NH_2	311	377	4
8	**14d**	2-indanyl	Bn	1,4-Me	$NHCH_2CO_2Et$	311	377	8
9	**14g**	Bn	Bn	1,4-Bn	$NHCH_2CO_2Et$	318	381	10
10	**14e**	2-indanyl	nPr	1,4-Bn	$NHCH_2CO_2Et$	316	382	4
11	**14f**	2-indanyl	nPr	1,4-Me	$NHCH_2CO_2Et$	313	380	5
12	**7a**	1-naphtyl	iBu	1,4-Bn	NMe_2	318	378	2
13	**7b**	phenethyl	Bn	1,4-iBu	NMe_2	316	378	5
14	**8a**	1-naphtyl	iBu	1,5-Bn	NMe_2	322	437	37
15	**8b**	phenethyl	Bn	1,5-iBu	NMe_2	320	422	51
16	**14h**	Bn	Bn	1,4-Bn	SCH_2CO_2Et	340	398	2

$\lambda_{abs,\ max}$ and $\lambda_{em,\ max}$ are the wavelengths of absorption and emission maxima, respectively, and Φ_F is the fluorescence quantum yield

doi:10.1371/journal.pone.0124423.t001

Fig 10. Photophysical characterization of 14b, 14f, 14g, 14h and 14i. Normalised absorption (solid lines) and emission (dashed lines) spectra of a selection of the investigated compounds (the full set of absorption and emission spectra can be found in the SI).

doi:10.1371/journal.pone.0124423.g010

The 8-triazolyl compounds (Table 1, entries 1–15) have absorption maxima in the range 310–322 nm, with the exception of **14h** (entry 16), which bears a sulphur substituent in the 6-position. The absorption maximum of this compound is redshifted to 340 nm. Compounds with a 6-dimethylamino substituent, such as R_4 and a 1,4-triazole, all have low fluorescence quantum yields between 1 and 2% (entries 1–5,12–13). Changing from tertiary to primary or secondary amines as R_4 substituent gives higher quantum yield (5–10%). A selection of absorption and emission spectra is shown in Fig 10.

The substitution pattern on the triazole and in the 9 and N2 position seems to have little effect on the quantum yield. This is expected since none of the substituents in these positions changes the conjugation of the heterocyclic core. Interestingly, changing the regioisomerism of the triazole from 1,4 to 1,5 (entries 12–15) results in a 10-20-fold increase of the quantum yield. In addition, the Stokes shift increases from 62 to 102 nm (entries 13 and 15). To the best of our knowledge, this is the first time this regioisomeric effect has been observed for fluorescent triazoles and it might have implications in the field of fluorescent base analogs. The increase in quantum yield observed when shifting from the 1,4 to the 1,5-regioisomer could possibly originate from increased steric hindrance and a higher rotational barrier of the purine-triazole bond leading to less rotational flexibility in the excited state, decreasing the rate of non-radiative deactivation. To establish the influence of the triazole on the fluorescent properties, **5a** and **15–16** bearing a proton, bromine, and an alkyne in the 8-position, respectively, were also measured (data not shown). These compounds all displayed very weak fluorescent properties and demonstrate that the 8-triazole substituent is necessary to observe the higher quantum yields.

Materials and Methods

A representative synthesis example of 6-(ethoxy-carbonyl-methylamino)-9-(2-indanyl)-8-(1-methyl-1H-1,2,3-triazol-4-yl)-2-(1-propylamino)purine (**14f**) is described below.

2-Amino-9-*tert*-butoxycarbonyl-6-chloropurine

Following a published procedure[29] with minor modifications, 2-amino-6-chloropurine (2.50 g, 14.7 mmol) and di-*tert*-butyl dicarbonate (3.21 g, 14.7 mmol) were dissolved in anhydrous DMSO (50 ml). The pale yellow solution was cooled in an ice bath with vigorous stirring and the ice bath was removed just as the DMSO started to freeze. DMAP (90 mg, 0.74 mmol) was added and the solution was stirred under nitrogen at room temperature for 8 h. Additional di-*tert*-butyl dicarbonate (220 mg, 1.00 mmol) was added and the reaction mixture was stirred at room temperature overnight. Full consumption of starting material and formation of one new spot was confirmed by TLC (10% methanol in $CHCl_3$).*The reaction mixture was* diluted with water (450 ml) and extracted with ethyl acetate (3 x 150 ml). The organic phases were washed with water (5 x 100 ml), dried over Na_2SO_4, filtered and evaporated to give the expected product as a white solid (3640 mg, 92%) which was used without further purification in the next step. ^{1}H NMR ($CDCl_3$): 8.13 (s, 1H), 5.92 (br s, 2H), 1.66 (s, 9H); ^{13}C NMR ($CDCl_3$): 160.6, 153.4, 152.4, 145.7, 140.2, 125.5, 87.2, 28.0.

2-*tert*-Butoxycarbonylamino-6-chloropurine (1)

Sodium hydride (715 mg, 17.9 mmol, 60% mineral oil dispersion) was added to a stirred solution of 2-amino-9-tert-butoxycarbonyl-6-chloropurine, (3490 mg, 12.9 mmol) in dry THF (120 ml) at room temperature under nitrogen. The white suspension was stirred at room temperature for 2 h. Full conversion of starting material was confirmed by TLC (70% ethyl acetate in pentane). The reaction was cooled to 0°C and quenched with brine (5 ml); a white precipitate was observed after the addition. The mixture was then allowed to reach room temperature. The THF was removed under reduced pressure (note: save 10–20 ml THF, to simplify the extraction). $CHCl_3$ (200 ml) and distilled water (800 ml) were added (everything did not dissolve). The pH on the aqueous phase was determined to be 14. The phases were separated and extracted with $CHCl_3$ (3 x 100 ml, note: wait approximately 10 min between every extraction) and these organic phases were discarded. Sat. $NaHCO_3$ (aq.) was added to the aqueous phase, whereupon a white precipitate was observed; the aqueous phase was extracted with $CHCl_3$ (3 x 100 ml). The combined organic phases were washed with brine. The solvent was removed under reduced pressure to yield **1** as a white solid in quantitative yield. ^{1}H and ^{13}C NMR corresponds with previously published results[27]. ^{1}H NMR ($CDCl_3$): 13.53 (s, 1H), 8.44 (s, 1H), 7.78 (s, 1H), 1.58 (s, 9H); ^{13}C NMR ($CDCl_3$): 153.3, 151.6, 151.3, 151.0, 145.5, 128.3, 82.4, 28.3.

General procedure A: Mitsunobu reaction in the 9-position

The alkylation was performed following a published procedure[29] with minor modifications. **1** (1.0 eq.) was dissolved in dry THF under nitrogen in oven-dried round-bottomed flask and alcohol (1.1–2.5 eq.) and PPh_3 (1.1–2.5 eq.) was added. The nitrogen flow was temporarily removed when solid alcohols were added. When all of the PPh_3 was dissolved, DIAD (1.0–2.5 eq.), were added drop wise. The reaction was stirred at room temperature under nitrogen, until TLC indicated full consumption of the starting material, unless otherwise noted. The solvent was removed under reduced pressure and the crude product was purified by flash column chromatography or automated flash column chromatography.

6-Chloro-9-(2-indanyl)-2-(*tert*-butoxycarbonylamino)purine (9a)

Compound **9a** was synthesised following general procedure A at 0°C for 2 h from **1** (816 mg, 3.03 mmol), 2-indanol (1031 mg, 7.60 mmol), PPh_3 (1953 mg, 7.44 mmol) and DIAD (1.45 ml, 7.36 mmol) as substrates in dry THF (42 ml). The crude product was purified by flash column

chromatography (30–70% ethyl acetate in pentane) to provide **9a** as a white solid (970 mg, 83%). ^{1}H NMR (CDCl$_3$): 7.73 (s, 1H), 7.53 (br s, 1H), 7.34–7.25 (m, 4H), 5.55 (tt, J 7.4, 4.3 Hz, 1H), 3.63 (dd, J 16.5, 7.4 Hz, 2H), 3.26 (dd, J 16.4, 4.3 Hz, 2H), 1.54 (s, 9H); ^{13}C NMR (CDCl$_3$): 152.6, 152.3, 151.1, 150.2, 141.9, 139.6, 127.6, 127.5, 124.8, 81.7, 55.0, 40.1, 28.2. HRMS m/z [M + H]$^+$ calculated for C$_{19}$H$_{20}$ClN$_5$O$_2$: 386.1384. Found: 386.1351.

General procedure B: Mitsunobu reaction in the 2-position

The alkylation was performed following a published procedure[29] with minor modifications. The purine was dissolved in dry THF under nitrogen in an oven-dried round-bottomed flask, PBu$_3$ (2.4–2.6 eq.), alcohol (2.4–2.6 eq.) and ADDP (2.5–2.6 eq.) was added in that order. The nitrogen flow was temporarily suspended when solid alcohols and ADDP were added. The reaction was stirred at room temperature, until TLC indicated full consumption of the starting material, unless otherwise noted. The obtained white precipitate was filtered off, and washed with THF, and the solvent was removed under reduced pressure. The crude product was purified by flash column chromatography or automated flash column chromatography.

6-Chloro-9-(2-indanyl)-2-(N-propyl-tert-butoxycarbonylamino)purine (10b)

Compound **10b** was synthesised following general procedure B from **9a** (2930 mg, 7.59 mmol), n-propanol (1.45 ml, 19.40 mmol), PBu$_3$ (4.8 ml, 18.26 mmol) and ADDP (4790 mg, 18.99 mmol) in dry THF (144 ml). The reaction was stirred at room temperature for 24 h. The reaction was monitored by TLC (50% ethyl acetate in pentane). The crude product was purified by flash column chromatography (25–100% ethyl acetate in pentane) to provide compound **10b** as a light yellow sticky solid (2450 mg, 75%). Starting material (727 mg) was recovered after column chromatography. ^{1}H NMR (CDCl$_3$): 7.84 (s, 1H), 7.33–7.24 (m, 4H), 5.45 (tt, J 7.6, 5.0 Hz, 1H), 3.89–3.85 (m, 2H), 3.60 (dd, J 16.3, 7.5 Hz, 3H), 3.36 (dd, J 16.3, 5.0 Hz, 2H), 1.67 (sext, J 7.5 Hz, 2H), 1.50 (s, 9H), 0.88 (t, J 7.5, 3H); ^{13}C NMR (CDCl$_3$): 155.3, 154.0, 152.4, 150.5, 142.8, 139.6, 128.4, 127.7, 124.9, 81.4, 55.5, 50.2, 39.8, 28.3, 22.2, 11.4. HRMS m/z [M + H]$^+$ calculated for C$_{22}$H$_{26}$ClN$_5$O$_2$: 428.1853. Found: 428.1865.

6-(Ethoxy-carbonyl-methylamino)-9-(2-indanyl)-2-(1-propylamino)purine (11e)

The reaction was run in two batches, which were then pooled prior to work-up and purification. **10b** (250 mg, 1.17 mmol) was suspended in ethanol (15 ml, 99.7%) in two oven-dried microwave vials. Glycine ethyl ester hydrochloride (245 mg, 1.76 mmol) and triethyl amine (0.41 ml, 2.94 mmol) were added and the reactions were heated to 100°C whereupon the starting materials dissolved. The reaction was left at 100°C overnight. TLC (5% methanol in CH$_2$Cl$_2$) indicated full consumption of the starting material. The two batches were pooled and the solvent was removed under reduced pressure. The crude product was dissolved in CH$_2$Cl$_2$ (13 ml), and TFA (4 ml) was added. The reaction mixture was stirred at room temperature for 3 h, after which full deprotection was confirmed by LCMS. The reaction mixture was cooled on ice and diluted with distilled water (20 ml) and then basified with 6 M NaOH (aq.). The aqueous phase was extracted with CH$_2$Cl$_2$ (4 x 20 ml). The combined organic phases were washed with brine and dried over MgSO$_4$, filtered, and the solvent was removed under reduced pressure. The crude product was purified by automated flash column chromatography (5% methanol in CH$_2$Cl$_2$) to provide compound **11e** as a light yellow oil/foam (451 mg, 98%). ^{1}H NMR (CDCl$_3$): 7.31 (s, 1H), 7.30–7.18 (m, 4H), 6.25 (br s, 1H), 5.24–5.31 (m, 1H), 4.86 (t, J 5.9 Hz,

1H), 4.31 (d, J 5.4 Hz, 2H), 4.20 (q, J 7.1 Hz, 2H), 3.50 (dd, J 16.2, 7.6 Hz, 2H), 3.38–3.25 (m, 4H), 1.59 (sext, J 7.3 Hz, 2H), 1.26 (t, J 7.1 Hz, 3H), 0.95 (t, J 7.4 Hz, 3H); ^{13}C NMR (CDCl$_3$): 170.7, 159.6, 154.5, 151.8, 140.5, 135.1, 127.2, 124.7, 114.4, 61.2, 54.2, 43.8, 42.7, 39.8, 23.2, 14.3, 11.7. HRMS m/z [M + H]$^+$ calculated for C$_{21}$H$_{25}$N$_6$O$_2$: 395.2195. Found: 395.2195.

General procedure D: 8-bromination of 2,6,9-substituted purines

Purine (1.0 eq.) was dissolved in dry CH$_2$Cl$_2$ in oven-dried glassware under nitrogen. The nitrogen flow was temporarily suspended when pyridinium tribromide (PyrBr$_3$) (1.1–1.4 eq.) was added in one portion. The reaction mixture was stirred at room temperature under nitrogen until full conversion was observed by TLC or LCMS. The reaction was quenched with 10% Na$_2$S$_2$O$_3$ (aq.); the colour changed from yellow to colorless. The pH was adjusted to 9–12 with 15% NaOH (aq.). The phases were separated and the aqueous phase was extracted with CH$_2$Cl$_2$ (x 3). The organic phases were pooled, washed with brine, dried over Na$_2$SO$_4$ and filtered. The solvent was removed under reduced pressure, and the crude product was purified by flash column chromatography.

8-Bromo-6-(ethoxy-carbonyl-methylamino)-9-(2-indanyl)-2-(1-propylamino)purine (12e)

Compound **12e** was synthesised following general procedure D from **11e** (418 mg, 1.06 mmol) and PyrBr$_3$ (410 mg, 1.21 mmol) in dry CH$_2$Cl$_2$ (17 ml). The reaction was stirred at room temperature for 5 h, whereupon full consumption of starting material was observed by LCMS. The crude product was purified by automated flash column chromatography (20–30% ethyl acetate in pentane) to provide **12e** as a colorless oil (479 mg, 96%). ^{1}H NMR (CDCl$_3$): 7.26–7.19 (m, 4H), 5.92 (t, J 5.3 Hz, 1H), 5.34 (quin, J 9.1 Hz, 1H), 4.77 (t, J 5.9 Hz, 1H), 4.30 (d, J 5.5 Hz, 2H), 4.23 (q, J 7.1 Hz, 2H), 3.96 (dd, J 15.5, 9.2 Hz, 2H), 3.26 (dd, J 15.4, 9.0 Hz, 2H), 3.14 (q, J 6.6 Hz, 2H), 1.48 (sext, J 7.4 Hz, 2H), 1.29 (t, J 7.1 Hz, 3H), 0.84 (t, J 7.4 Hz, 3H); ^{13}C NMR (CDCl$_3$): 170.5, 158.8, 153.4, 153.1, 140.8, 126.9, 124.5, 122.2, 115.3, 61.4, 56.6, 43.6, 42.6, 37.0, 23.0, 14.4, 11.6. HRMS m/z [M + H]$^+$ calculated for C$_{21}$H$_{25}$BrN$_6$O$_2$: 473.1300. Found: 473.1331.

6-(Ethoxy-carbonyl-methylamino)-8-ethynyl-9-(2-indanyl)-2-(1-propylamino)purine (13e)

PdCl$_2$(PPh$_3$)$_2$ (28 mg, 0.040 mmol), CuI (31 mg, 0.16 mmol), and amberlite IRA-67 (718 mg, 4.02 mmol) were added to a solution of **12e** (380 mg, 0.803 mmol) in dry THF (12 ml). The vial was capped, nitrogen was bubbled through the reaction mixture and ethynyltrimethylsilane (450 μl, 3.25 mmol) was added. The yellow reaction mixture was heated in a microwave reactor at 110°C for 50 min. Full consumption of **12e** was confirmed by TLC (2% methanol in CHCl$_3$). The reaction mixture was filtered through a short plug of silica that was eluted with THF. The solution was concentrated and the volume was adjusted to 8 ml. Polymer-supported fluoride (422 mg) was added and the reaction mixture was stirred under nitrogen at room temperature for 19 h. The polymer was filtered off, washed with THF and CH$_2$Cl$_2$ and the solvents were removed under reduced pressure. Purification by flash column chromatography (first column eluted with 2% methanol in CH$_2$Cl$_2$ and second column with 33% ethyl acetate in pentane) provided **13e** as a yellow solid (200 mg, 60%). ^{1}H NMR (CDCl$_3$): 7.26–7.17 (m, 4H), 6.11 (s, 1H), 5.47 (quin, J 9.0 Hz, 1H), 4.84 (t, J 5.8 Hz, 1H), 4.31 (br s, 2H), 4.23 (q, J 7.1 Hz, 2H), 3.91 (dd, J 15.5, 9.3 Hz, 2H), 3.35 (s, 1H), 3.30 (dd, J 15.5, 8.8 Hz, 3H), 3.20 (q, J 6.7 Hz, 2H), 1.51 (sext, J 7.3 Hz, 2H), 1.28 (t, J 7.1 Hz, 3H), 0.87 (t, J 7.4 Hz, 3H); ^{13}C NMR (CDCl$_3$): 170.4,

159.9, 154.4, 151.7, 141.0, 129.7, 126.9, 124.5, 114.8, 83.0, 74.3, 61.4, 55.4, 43.6, 42.6, 37.6, 23.1, 14.3, 11.6. HRMS m/z [M + H]$^+$ calculated for $C_{23}H_{26}N_6O_2$: 419.2195. Found: 419.2206.

6-(Ethoxy-carbonyl-methylamino)-9-(2-indanyl)-8-(1-methyl-1H-1,2,3-triazol-4-yl)-2-(1-propylamino)purine (14f)

Methyl iodide (24 µl, 0.39 mmol) and sodium azide (25 mg, 0.38 mmol) in dry DMF (2 ml) were stirred at room temperature for 3 h in a microwave vial. The formed methyl azide solution was then transferred to a microwave vial containing **13e** (82 mg, 0.20 mmol), sodium ascorbate (12 mg, 0.06 mmol), CuI (7 mg, 0.04 mmol) and DMEDA (5 µl, 0.05 mmol) in dry DMF (1.5 ml). The reaction mixture was heated at 60°C for 3 h and then at room temperature for 15 h. Full consumption of **13e** was confirmed by TLC (10% methanol in CHCl$_3$). The reaction mixture was poured into ethyl acetate (25 ml), extracted with water (3 x 20 ml), dried over Na$_2$SO$_4$ and the solvents were removed under reduced pressure. *Caution*: *Keep aqueous phase slightly basic (0.5 M NaOH (aq.) was added to the aqueous phase) to avoid hydrazoic acid formation*. Purification by flash column chromatography (ethyl acetate) provided **14f** as a yellow solid (81 mg, 87%). ^{1}H NMR (CDCl$_3$): 8.11 (br s, 1H), 7.25–7.13 (m, 4H), 6.31 (br s, 1H), 6.16 (br s, 1H), 4.75 (br s, 4.75, 1H), 4.33 (s, 2H), 4.24 (q, *J* 7.1 Hz, 2H),4.14 (s, 3H), 4.05 (dd, *J* 14.9, 8.5 Hz, 2H), 3.32 (dd, *J* 14.8, 8.9 Hz, 2H), 3.12 (q, *J* 6.6 Hz, 2H), 1.46 (q, *J* 7.2 Hz, 1H), 1.30 (t, *J* 7.0 Hz, 3H), 0.81 (t, *J* 7.4 Hz, 3H); ^{13}C NMR (CDCl$_3$): 170.9, 158.9, 154.4, 153.4, 141.6, 140.9, 139.0, 126.5, 125.4, 124.4, 114.7, 61.2, 56.1, 43.6, 42.5, 37.2, 36.8, 23.0, 14.3, 11.5. *Note*: *Weighting functions were applied to the ^{1}H NMR spectra to obtain J couplings (sine bell: 2°, sine square: 88°)*. HRMS m/z [M + H]$^+$ calculated for $C_{24}H_{29}N_9O_2$: 476.2522. Found: 476.2485.

Conclusion

An efficient strategy for the preparation of 2,6,9-substituted 8-triazolylpurines has been developed. The target compounds are obtained in excellent yields by a convenient multistep procedure. Conformation studies by solution phase NMR spectroscopy demonstrated that 2,6,9-substituted 8-triazolylpurines could mimic the topography of an α-helix and could be potentially useful as MDM2/p53 inhibitors. However, our study clearly indicates that this is not sufficient for *in vitro* activity as the first series of compounds were inactive at the tested concentrations in a biochemical fluorescence polarisation assay targeting MDM2/p53. Further iterative design-synthesis-testing cycles using docking as the main design tool resulted in a one micromolar inhibitor (**14f**, 10 µM). Binding of **14f** to MDM2 was confirmed by WaterLOGSY measurements. Furthermore, the 2,6,9-substituted 8-triazolylpurines displayed moderate to high fluorescence quantum yields in the range of 5–51%. The combination of fluorescent properties with inhibitory effect on the MDM2-p53 interaction could potentially be useful for real-time imaging as well as for the development of *in vitro* displacement assays for MDM2/p53. Developments in this direction are currently ongoing in our laboratories.

Supporting Information

S1 File. Describes synthesis and characterisation including Proton (^{1}H) and Carbon (^{13}C) NMR spectra of all compounds synthesised. In addition, experimental procedures for the biological evaluation and photophysical characterisation are included. A more specific table of contents can be located in this document.
(PDF)

Acknowledgments

Author Contributions

Conceived and designed the experiments: MP DB JM MG. Performed the experiments: MP DB JRN JJ LI JM. Analyzed the data: MP DB JJ JRN JM LI RKG RWK JA MG. Contributed reagents/materials/analysis tools: RKG RWK JA MG. Wrote the paper: MP DB MG.

References

1. Stites WE. Protein—Protein Interactions: Interface Structure, Binding Thermodynamics, and Mutational Analysis. Chem. Rev. 1997; 97: 1233–1250. PMID: 11851449

2. Jones S, Thornton JM. Principles of protein-protein interactions. P. Natl. Acad. Sci. USA 1996; 93: 13–20.

3. Keskin O, Gursoy A, Ma B, Nussinov R. Principles of Protein—Protein Interactions: What are the Preferred Ways For Proteins To Interact? Chem. Rev. 2008; 108: 1225–1244. doi: 10.1021/cr040409x PMID: 18355092

4. Jochim AL, Arora PS. Systematic Analysis of Helical Protein Interfaces Reveals Targets for Synthetic Inhibitors. ACS Chem. Biol. 2010; 5: 919–923. doi: 10.1021/cb1001747 PMID: 20712375

5. Vousden KH, Prives C. Blinded by the Light: The Growing Complexity of p53. Cell 2009; 137: 413–431. doi: 10.1016/j.cell.2009.04.037 PMID: 19410540

6. Vogelstein B, Lane D, Levine AJ. Surfing the p53 network. Nature 2000; 408: 307–310. PMID: 11099028

7. Kussie PH, Gorina S, Marechal V, Elenbaas B, Moreau J, et al. Structure of the MDM2 Oncoprotein Bound to the p53 Tumor Suppressor Transactivation Domain. Science 1996; 274: 948–953. PMID: 8875929

8. Aeluri M, Chamakuri S, Dasari B, Guduru SKR, Jimmidi R, Jogula S, et al. Small Molecule Modulators of Protein—Protein Interactions: Selected Case Studies. Chem. Rev. 2014; 114: 4640–4694. doi: 10.1021/cr4004049 PMID: 24673632

9. Azzarito V, Long K, Murphy NS, Wilson AJ. Inhibition of [alpha]-helix-mediated protein-protein interactions using designed molecules. Nat. Chem. 2013; 5: 161–173. doi: 10.1038/nchem.1568 PMID: 23422557

10. Vassilev LT, Vu BT, Graves B, Carvajal D, Podlaski F, Filipovic Z, et al. In Vivo Activation of the p53 Pathway by Small-Molecule Antagonists of MDM2. Science 2004; 303: 844–848. PMID: 14704432

11. Sun D, Li Z, Rew Y, Gribble M, Bartberger MD, Beck HP, et al. Discovery of AMG 232, a Potent, Selective, and Orally Bioavailable MDM2–p53 Inhibitor in Clinical Development. J. Med. Chem. 2014; 57: 1454–1472. doi: 10.1021/jm401753e PMID: 24456472

12. Zhao Y, Yu S, Sun W, Liu L, Lu J, McEachern D, et al. A Potent Small-Molecule Inhibitor of the MDM2–p53 Interaction (MI-888) Achieved Complete and Durable Tumor Regression in Mice. J. Med. Chem 2013; 56: 5553–5561. doi: 10.1021/jm4005708 PMID: 23786219

13. Orner BP, Ernst JT, Hamilton AD. Toward Proteomimetics: Terphenyl Derivatives as Structural and Functional Mimics of Extended Regions of an α-Helix. J. Am. Chem. Soc. 2001; 123: 5382–5383. PMID: 11457415

14. Yin H, Lee G-i, Park HS, Payne GA, Rodriguez JM, Sebti SM, et al. Terphenyl-Based Helical Mimetics That Disrupt the p53/HDM2 Interaction. Angew. Chem. Ger. Edit. 2005; 117: 2764–2767.

15. Lee JH, Zhang Q, Jo S, Chai SC, Oh M, Im W, et al. Novel Pyrrolopyrimidine-Based α-Helix Mimetics: Cell-Permeable Inhibitors of Protein—Protein Interactions. J. Am. Chem. Soc. 2010; 133: 676–679.

16. Rosemeyer H. The Chemodiversity of Purine as a Constituent of Natural Products. Chem. Biodivers. 2004; 1: 361–401. PMID: 17191854

17. Horton DA, Bourne GT, Smythe ML. The Combinatorial Synthesis of Bicyclic Privileged Structures or Privileged Substructures. Chem. Rev. 2003; 103: 893–930. PMID: 12630855

18. Dyrager C, Börjesson K, Dinér P, Elf A, Albinsson B, Wilhelmsson M, et al. Synthesis and Photophysical Characterisation of Fluorescent 8-(1H-1,2,3-Triazol-4-yl)adenosine Derivatives. Eur. J. Org. Chem. 2009; 2009: 1515–1521.

19. Dierckx A, Dinér P, El-Sagheer AH, Kumar JD, Brown T, Grøtli M, et al. Characterization of photophysical and base-mimicking properties of a novel fluorescent adenine analogue in DNA. Nucleic Acids Res. 2011; 39: 4513–4524. doi: 10.1093/nar/gkr010 PMID: 21278417

20. Pedersen DS, Abell A. 1,2,3-Triazoles in Peptidomimetic Chemistry. Eur. J. Org. Chem. 2011; 2011: 2399–2411.

21. Davis MR, Singh EK, Wahyudi H, Alexander LD, Kunicki JB, Nazarova LA, et al. Synthesis of sansalvamide A peptidomimetics: triazole, oxazole, thiazole, and pseudoproline containing compounds. Tetrahedron 2012; 68: 1029–1051. PMID: 22287031

22. Horne WS, Yadav MK, Stout CD, Ghadiri MR. Heterocyclic Peptide Backbone Modifications in an α-Helical Coiled Coil. J. Am. Chem. Soc. 2004; 126: 15366–15367. PMID: 15563148

23. Meldal M, Tornøe CW. Cu-Catalyzed Azide-Alkyne Cycloaddition. Chem. Rev. 2008; 108: 2952–3015. doi: 10.1021/cr0783479 PMID: 18698735

24. Zhang L, Chen XG, Xue P, Sun HH, Williams ID, Sharpless KB, et al. Ruthenium-catalyzed cycloaddition of alkynes and organic azides. J. Am. Chem. Soc. 2005; 127: 15998–15999. PMID: 16287266

25. Kwok SW, Fotsing JR, Fraser RJ, Rodionov VO, Fokin VV. Transition-Metal-Free Catalytic Synthesis of 1,5-Diaryl-1,2,3-triazoles. Org. Lett. 2010; 12: 4217–4219. doi: 10.1021/ol101568d PMID: 20825167

26. Chang Y-T, Gray NS, Rosania GR, Sutherlin DP, Kwon S, et al. Synthesis and application of functionally diverse 2,6,9-trisubstituted purine libraries as CDK inhibitors. Chem. Biol. 1999; 6: 361–375. PMID: 10375538

27. Bliman D, Pettersson M, Bood M, Grøtli M. 8-Bromination of 2,6,9-trisubstituted purines with pyridinium tribromide. Tetrahedron Lett. 2014; 55: 2929–2931.

28. Fletcher S, Shahani VM, Lough AJ, Gunning PT. Concise access to N9-mono-, N2-mono- and N2,N9-di-substituted guanines via efficient Mitsunobu reactions. Tetrahedron 2010; 66: 4621–4632.

29. Fletcher S, Shahani VM, Gunning PT. Facile and efficient access to 2,6,9-tri-substituted purines through sequential N9, N2 Mitsunobu reactions. Tetrahedron Lett. 2009; 50: 4258–4261.

30. Čechová L, Jansa P, Šála M, Dračínský M, Holý A, Janeba Z. The optimized microwave-assisted decomposition of formamides and its synthetic utility in the amination reactions of purines. Tetrahedron 2011; 67: 866–871.

31. Johansson JR, Lincoln P, Nordén B, Kann N. Sequential One-Pot Ruthenium-Catalyzed Azide—Alkyne Cycloaddition from Primary Alkyl Halides and Sodium Azide. J. Org. Chem. 2011; 76: 2355–2359. doi: 10.1021/jo200134a PMID: 21388208

32. Cicero DO, Barbato G, Bazzo R. NMR Analysis of Molecular Flexibility in Solution: A New Method for the Study of Complex Distributions of Rapidly Exchanging Conformations. Application to a 13-Residue Peptide with an 8-Residue Loop. J. Am. Chem. Soc. 1995; 117: 1027–1033.

33. Koivisto JJ, Kumpulainen ETT, Koskinen AMP. Conformational ensembles of flexible [small beta]-turn mimetics in DMSO-d6. Org. Biomol. Chem. 2010; 8: 2103–2116. doi: 10.1039/b921794k PMID: 20401387

34. Fridén-Saxin M, Seifert T, Hansen LK, Grøtli M, Erdelyi M, Luthman K. Proline-mediated formation of novel chroman-4-one tetrahydropyrimidines. Tetrahedron 2012; 68: 7035–7040.

35. Danelius E, Brath U, Erdélyi M. Insight into β-Hairpin Stability: Interstrand Hydrogen Bonding. Synlett. 2013; 24: 2407–2410.

36. Gonzalez-Lopez de Turiso F, Sun D, Rew Y, Bartberger MD, Beck HP, Canon J, et al. Rational Design and Binding Mode Duality of MDM2–p53 Inhibitors. J. Med. Chem. 2013; 56: 4053–4070. doi: 10.1021/jm400293z PMID: 23597064

37. Michelsen K, Jordan JB, Lewis J, Long AM, Yang E, Rew Y. Ordering of the N-Terminus of Human MDM2 by Small Molecule Inhibitors. J. Am. Chem. Soc. 2012; 134: 17059–17067. doi: 10.1021/ja305839b PMID: 22991965

38. Rew Y, Sun D, Gonzalez-Lopez De Turiso F, Bartberger MD, Beck HP, Canon J, et al. Structure-Based Design of Novel Inhibitors of the MDM2–p53 Interaction. J. Med. Chem. 2012; 55: 4936–4954. doi: 10.1021/jm300354j PMID: 22524527

39. Dalvit C, Fogliatto G, Stewart A, Veronesi M, Stockman B. WaterLOGSY as a method for primary NMR screening: Practical aspects and range of applicability. J. Biomol. NMR 2001; 21: 349–359. PMID: 11824754

40. Bharatham N, Bharatham K, Shelat AA, Bashford D. Ligand Binding Mode Prediction by Docking: Mdm2/Mdmx Inhibitors as a Case Study. J. Chem. Inf. Model. 2013; 54: 648–659.